A VISCOELASTIC MODEL FOR THE RESPONSE OF A STEP CHANGE IN VELOCITY OF THE HUMAN OTOLITH ORGANS

by

John Rowland Cotton

Thesis submitted to the Faculty of the
Virginia Polytechnic Institute and State University
in partial fulfillment of the requirements for the degree of
MASTER OF SCIENCE
in
Engineering Mechanics

Approved:

J. Wallace Grant

Daniel J. Schneck

George W. Swift

November 1989

Blacksburg, Va.

A VISCOELASTIC MODEL FOR THE RESPONSE OF A STEP CHANGE IN VELOCITY OF THE HUMAN OTOLITH ORGANS

by

John R. Cotton

Committee Chairman: J. Wallace Grant

Engineering Science and Mechanics

(Abstract)

The otolith organs are housed in the inner ear and are responsible for sensing accelerations and gravity. These inertial sensing systems are modeled in this thesis as a three material system consisting of a rigid otoconial plate attached to the skull by a gel layer, surrounded by a viscous endolymph fluid. The gel layer is considered to be a viscoelastic solid, and modeled as a simple Kelvin element. The governing differential equations are derived and nondimensionalized, yielding three nondimensional parameters: nondimensional density, R, nondimensional viscosity, M, and nondimensional elasticity, ϵ. The equations are solved using finite difference techniques on a digital computer. By comparing the model's response with previous biological research, values for the nondimensional parameters are found. The value of R is 0.75 and the value of ϵ is between 0.3 and 0.075. While the value of M is placed between 5. and 10., results indicate that to properly model the long time response of the otolith, a single and constant value for viscosity is not feasible.

Acknowledgements

I would like to thank the following persons for all their help, without which, this thesis would not be here now:

First and foremost, my parents, who instilled in me the love of learning, and were a continuous source of support when things got tough.

Dr. Grant, for his ideas, direction, and most of all patience. He was always there when I finished playing politics and was ready to get back to work.

, for all her aid with unfamiliar, and frequently unfriendly, computer systems.

Dr. Richard Roby, who made me realize that it was alot easier to write this thesis, than to sit through another lecture from him on how I should "just get it done".

Lastly, I would like to thank the Ton–80 Club and Jimmy Buffet, for helping me keep it all in perspective.

Table of Contents

1 Introduction 1

1.1 Anatomy and Physiology 2

1.2 Previous Models 6

2 Governing Equations 8

2.1 Gelatinous Layer 8

2.1.1 *The Gel as a Viscoelastic Material* 10

2.2 Plate and Fluid Layers 11

2.3 Nondimensionalization 11

3 Solution for a Step Change in Skull Velocity 14

3.1 Finite Difference Solution 14

3.1.1 *Time and Space Derivative Analogues* 16

3.1.2 *Displacement Calculations* 16

3.1.3 *Finite Difference Governing Equations* 16

3.1.4 *Solution Strategy* 20

3.2 Validation 20

4 Results 23

5 Discussion 30

6 Conclusions 33

Chapter 1
Introduction

Dating back to the times of ancient Greece, philosophers, doctors, scientists, and teachers have discussed the properties of the five senses: seeing, hearing, smelling, feeling, and tasting. It is through these senses that we gather information about our environment which we need for our very survival.

However there was always one sense that all have consistently neglected— the ability to sense motion and accelerations. It is easy to understand why this "sixth sense" has been neglected throughout history. Being housed deep within the inner ear, the vestibular system was not as readily observed as eyes, noses, and the like. Also, by its secure location and small size, it was not as susceptible to a localized injury that would provide a connection between the damage to the inner ear and a loss of balance or motion sensing. But most of all, until the twentieth century, the high rotational and linear accelerations made possible by modern technology were not experienced, and consequently this sense was taken for granted.

Today, we subject pilots and astronauts to accelerations that exceed anything in which the human organism evolved. Consequently, we begin to see problems that are unique throughout history. Astronauts experiencing motion sickness miss much of their mission time, physically unable to work. Pilots— having thousands of hours of flying time frequently become disoriented by even the simplest of turns and need to rely on instuments to distinguish up from down.

With the modern importance of the motion sensing organs, comes an interest in the study of their function. We know that the vestibular system is divided into the semicircular canals, which detect rotational movement, and the otoliths, which detect linear movements and respond to gravity.

The purpose of this thesis will be to develop a mathematical model of the otoconial organs and to study their response. By adjusting the response of the model to match observed results, it is hoped that insight might be gained into the physical properties of the

otolith.

This brief introduction will be followed by an introduction to the basic anatomy and physiology of the otoliths. A short review of previous models will follow.

Chapter 2 will cover the derivations of the governing equations while chapter 3 will discuss the computational solution of these equations for a step change in velocity. Chapter 4 will present the results of the model. Chapter 5 discusses the results, while chapter 6 will conclude the results.

1.1 Anatomy and Physiology

The otolith organs are located within the bony labyrinth of the temporal bone of the skull. This labyrinth, as shown in figure 1–1, contains, in addition to the otoliths, the semicircular canals, the cochlea, and other structures critical to hearing and motion sensing.

There are two separate otolith organs per ear. These are the utricle, which lies primarilly in the horizontal plane (parallel to the floor), and the saccule which is oriented in the medial plane (the plane of symmetry of your face). The saccule therefore is perpendicular to the utricle and for good reason. Each otolith is responsible for detecting gravitational forces and accelerations that exist in its respective plane. A top view of both the utricle and saccule is shown in figure 1–2.

The otoliths themselves consist of a viscoelastic gel, called the gel layer, which is connected to the skull at its base, and is imbedded with a weblike array of dense calcium carbonate crystals in its upper strata. This calcium carbonate crystal layer is $15 - 20\mu m$ thick and is called the otoconial membrane or otoconial layer. The otolith itself projects roughly $30 - 40\mu m$ into a cavity at least one millimeter in height which is filled with an endolymphatic fluid. Hair-like bundles of cilia protrude from nerve cells in the skull into the bottom layers of the gelatinous layer. Figure 1–3 is a cross section of an otolith organ showing these discrete parts.

When the skull is accelerated in a direction parallel to the otolith organ the inertial lag of the denser otolith crystals causes a deformation in the gel layer. This deformation results in a likewise deformation or bending of the cilia. The nerve cells transduce the deformation into an action potential which is carried to the central nervous system.

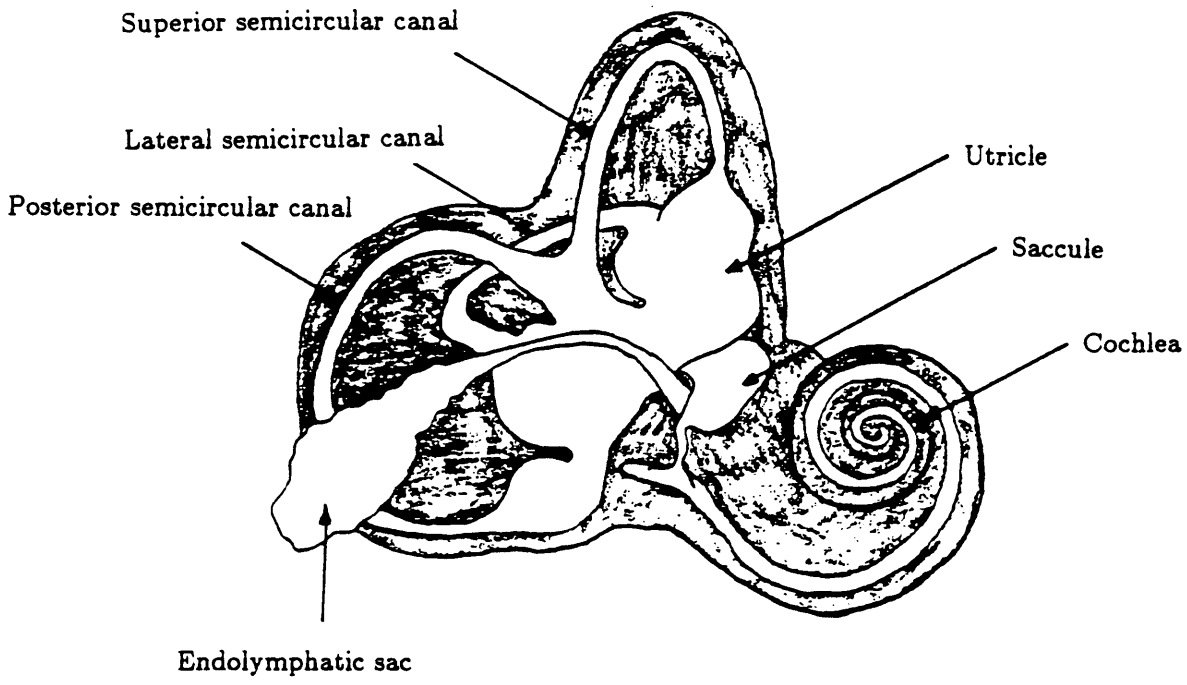

Figure 1-1: Bony Labyrinth of the Inner Ear

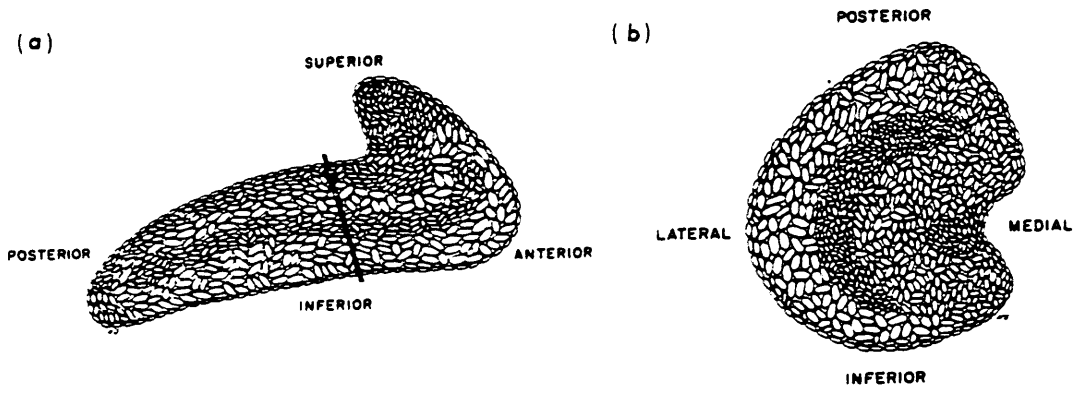

Figure 1-2: The otolith organs, saccule (a), and utricle (b).

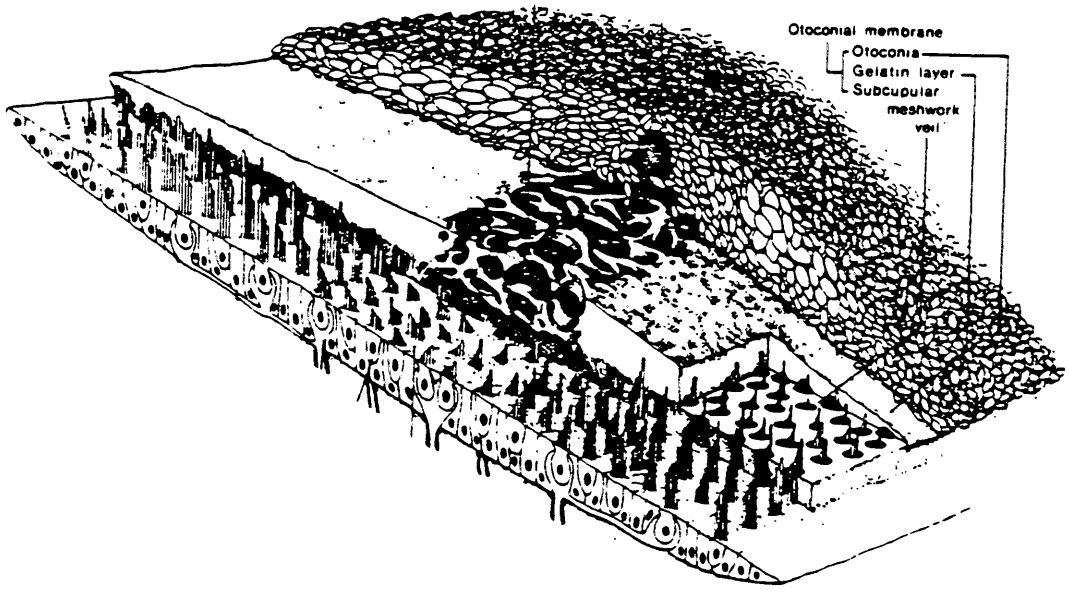

Figure 1-3: Cross section of the otolith organ

1.2 Previous Models

Previous work of Grant, Best, and LoNigro [7] modeled the otoliths as a system of three homogenous isotropic materials; the fluid, the gel, and the plate. Each material maintained a constant height and end effects were neglected. The simplified model is shown in figure 1–4. This work modeled the gel layer as a linearly elastic material. The material was in simple shear causing a linear profile of deformation.

This model produced displacements that far exceeded expected results. For reasonable values of elasticity, the otoconial plate would displace several times its height. Such large displacements would almost certainly cause permanent damage to the material. Also, when the elasticity was increased to provide smaller displacements, the system would oscillate. Since a person who is accelerated in one direction perceives motion to be unidirectional and decreasing, rather than a variable sensation that changes directions, we would expect an overdamped, not underdamped response. Therefore, we consider the oscillatory response to be in error.

The solution of this error is to include the effects of viscosity in the solid. By making the gel viscoelastic, the displacements should be reduced, and the long term effects would be stretched out further into time.

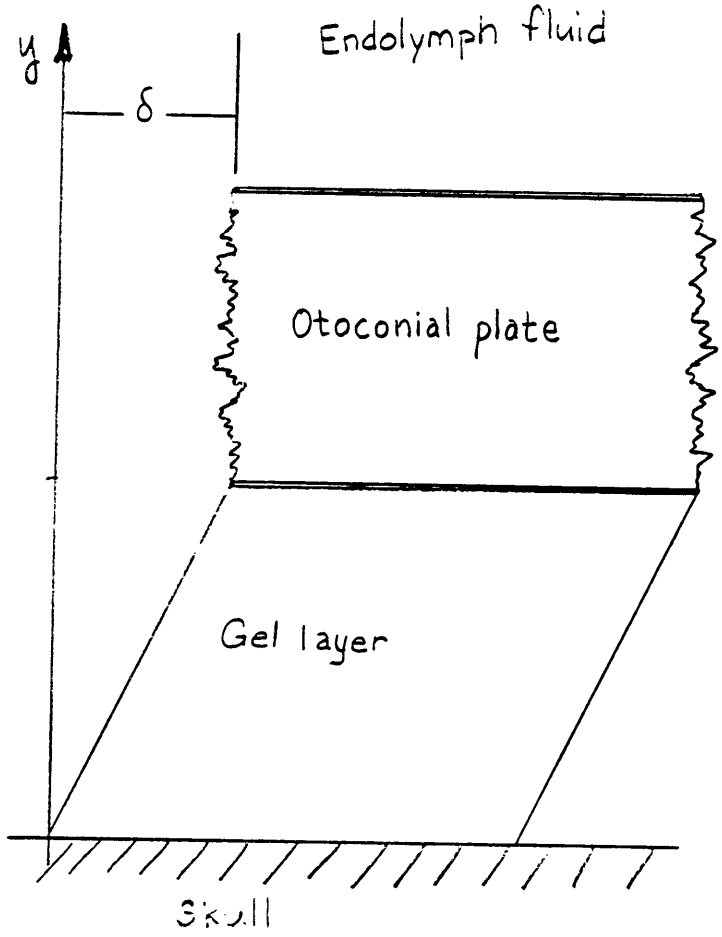

Figure 1-4: Simplified model of the otolith.

Chapter 2
Governing Equations

The basic formulation of this problem begins as the did the previous work of Grant, Best, and LoNigro [7]. The system will be treated as three separate parts; the endolymphatic fluid, the rigid plate of crystals, and the gel layer which will be modeled as a viscoelastic material. It is hoped that this new introduction of viscoelasticity into the problem will correct previous results. For each of the three components the free-body diagram will be drawn, and its governing equations will be derived.

Because the length and width of the otoconial membrane are several orders of magnitude larger than the height, the end effects on the plate will be neglected. The problem then approximates an infinite plate on top of an infinite gel under a viscous fluid.

2.1 Gelatinous Layer

The gelatinous layer will be considered as homogenous. The effects of the sensory cilia, which are encapsulated in fluid filled cavities within the gel layer, will be neglected, as with Grant, et. al. [7]. This should not affect the analysis much since these cilia assemblies only project into the bottom most portion of the gel.

In figure 2–1, the free body diagram of an element of the gel in shear can be seen. The forces acting on the section are the shear force on the top and bottom layers, τ_{y+dy} and τ_y, the pressure on both sides of the element, P_x and P_{x+dx}, and the body force on the element due to the component of gravity in the x direction, g_x. Using Newton's second law, $F = ma$, we can write,

$$\rho_{gel} dV \frac{\partial W}{\partial t} = (\tau_{y+dy} - \tau_y) dA + (P_x - P_{x+dx}) dy dz + dV \rho_{gel} g_x,$$

where ρ_{gel} is the density of the gel and W is the gel velocity with respect to an inertial reference frame.

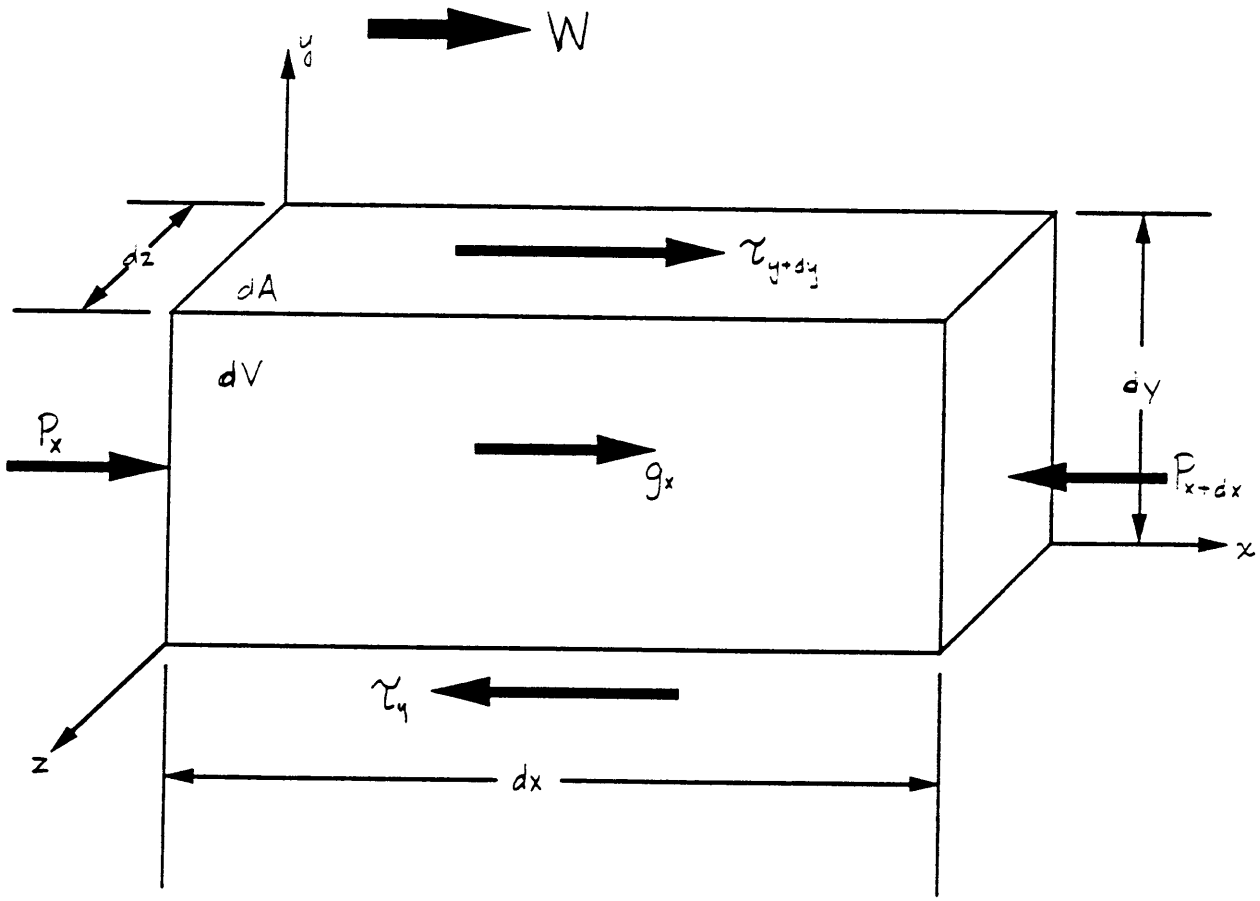

Figure 2-1: Free Body Diagram of Gel Element

By simply dividing through by space coordinates and substituting differential notation for the differences in shear and pressure, as well as substituting the endolymph fluid density for the gel density since $\rho_{gel} = \rho_f$, we arrive at,

$$\rho_f \frac{\partial W}{\partial t} = \rho_{gel} g_x - \frac{\partial P}{\partial x} + \frac{\partial \tau}{\partial y}.$$

The pressure gradient in a closed container is taken from Grant, et. al. [7] to be,

$$\frac{\partial P}{\partial x} = \rho_f (g_x - \frac{\partial V_s}{\partial t}),$$

where V_s is the skull velocity. Next we substitute the inertial gel velocity W with a velocity relative to the skull w defined as

$$w = W - V_s.$$

Substituting this back into the previous equation we arrive at

$$\rho_f \frac{\partial w}{\partial t} = \frac{\partial \tau}{\partial y}. \tag{2.1}$$

2.1.1 The Gel as a Viscoelastic Material

Now our model turns to adressing the nature of the shear force in the gel. Most gels, especially bio-gels, are of a viscoelastic nature. As mentioned, previous work by Grant, Best, and LoNigro [7], which modeled the gel as purely elastic, resulted in deformations much larger than expected for realistic values of elasticity. By treating the gel as a viscoelastic material the motion will be damped and the model will more closely resemble reality.

The Kelvin-Voight model for viscoelastic materials is sufficient for our purposes. Shear stress is a function of both displacement and velocity in a way analogous to a spring and a dashpot linked in parallel. Hence, the shear stress is expressed as,

$$\tau_{xy} = G \frac{\partial \delta}{\partial y} + \mu_{gel} \frac{\partial w}{\partial y}, \tag{2.2}$$

where G is the shear modulus, δ is the displacement, and μ_{gel} is the gel viscosity.

By substituting into the equation (2.2) for δ,

$$\delta = \int_0^t w(y,t)\, dt,$$

we get that,

$$\tau_{xy} = G \int_0^t \frac{\partial w}{\partial y}\, dt + \mu_s \frac{\partial w}{\partial y}.$$

By substituting this result into equation (2.1), the result is,

$$\rho_f \frac{\partial w}{\partial t} = G \int_0^t \frac{\partial^2 w}{\partial y^2}\, dt + \mu_{gel} \frac{\partial^2 w}{\partial y^2}. \qquad (2.3).$$

2.2 Plate and Fluid Layers

The governing equation for the otoconial plate is identical to the earlier work of Grant, Best, and LoNigro [7], with the addition of an term arising from the viscous effect of the gel. The forces considered in their analysis are illustrated in a free body diagram of the plate in figure 2–2.

The shear stress experienced at the plate which is caused by the gel, depicted in figure 2–2 as τ_g, is

$$\tau_g = G \int_0^t \frac{\partial w}{\partial y} dt + \mu_s \frac{\partial w}{\partial y},$$

which consists of the elastic shear stress (the first term) and the viscous shear stress (the second term). Therefore, to arrive at the plate governing equation, the addition of the second term from the equation above into the plate equation of Grant, et. al. [7], is sufficient.

$$\rho_o b \frac{\partial v}{\partial t} + (\rho_o - \rho_f) b [\frac{\partial V_s}{\partial t} - g_x] = \mu_f \frac{\partial u}{\partial y} - G \int_0^t \frac{\partial w}{\partial y} dt - \mu_s \frac{\partial w}{\partial y}. \qquad (2.4)$$

The fluid governing equation, which is derived from the linear version of Navier-Stokes equation,

$$\rho_f \frac{\partial U}{\partial t} = \rho_f g_x - \frac{\partial P}{\partial x} + \mu_f \frac{\partial^2 U}{\partial y^2},$$

is given by Grant, Best, and LoNigro [7] as,

$$\rho_f \frac{\partial u}{\partial t} = \mu_f \frac{\partial^2 u}{\partial y^2}. \qquad (2.5)$$

2.3 Nondimensionalization

From the previous sections we find the governing equations to be for the gel,

$$\rho_f \frac{\partial w}{\partial t} = G \int_0^t \frac{\partial^2 w}{\partial y^2}\, dt + \mu_{gel} \frac{\partial^2 w}{\partial y^2}, \qquad (2.3)$$

for the plate,

$$\rho_o b \frac{\partial v}{\partial t} + (\rho_o - \rho_f) b [\frac{\partial V_s}{\partial t} - g_x] = \mu_f \frac{\partial u}{\partial y} - G \int_0^t \frac{\partial w}{\partial y} dt - \mu_s \frac{\partial w}{\partial y}, \qquad (2.4)$$

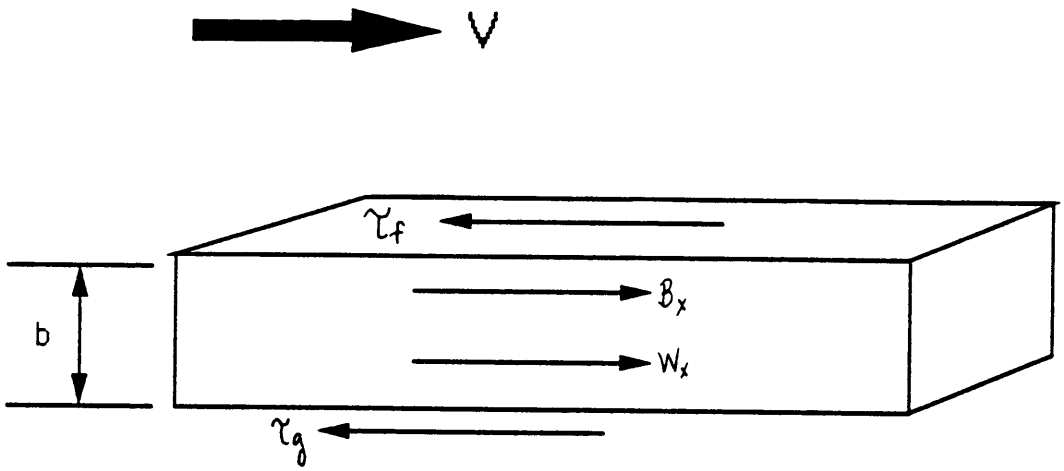

Figure 2-2: Free Body diagram of the otoconial plate

and for the fluid,

$$\rho_f \frac{\partial u}{\partial t} = \mu_f \frac{\partial^2 u}{\partial y^2}. \tag{2.5}$$

We begin by introducing nondimensionalized space $\bar{y}$, time $\bar{t}$,and velocities $\bar{u}$,$\bar{v}$, $\bar{w}$, and $\bar{V}_s$ These are defined as

$$\bar{y} = \frac{y}{b},$$

$$\bar{t} = \frac{\mu_f}{\rho_o b^2} t,$$

and

$$\bar{u} = \frac{u}{V},\ \bar{v} = \frac{v}{V},\ \bar{w} = \frac{w}{V},\ \text{and}\ \bar{V}_s = \frac{\bar{V}_s}{V},$$

where V is some characteristic velocity of the problem, after Grant, et. al. [7]. By introducing these nondimensionalized variables, the governing equations become

$$R\frac{\partial \bar{u}}{\partial \bar{t}} = \frac{\partial^2 \bar{u}}{\partial \bar{y}^2},$$

$$\frac{\partial \bar{v}}{\partial \bar{t}} + (1-R)[\frac{\partial \bar{V}_s}{\partial \bar{t}} - \bar{g}_x] = \frac{\partial \bar{u}}{\partial \bar{y}} - \epsilon \int_0^{\bar{t}} \frac{\partial \bar{w}}{\partial \bar{y}} \partial \bar{t} - M\frac{\partial \bar{w}}{\partial \bar{y}},$$

and

$$R\frac{\partial \bar{w}}{\partial \bar{t}} = \epsilon \int_0^{\bar{t}} \frac{\partial^2 \bar{w}}{\partial \bar{y}^2} \partial \bar{t} + M\frac{\partial^2 \bar{w}}{\partial \bar{y}^2},$$

where the the nondimensional parameters R, ϵ, and M, representing, in order, nondimensionalized density, elasticity, and viscosity, are defined as

$$R = \frac{\rho_f}{\rho_o},$$

$$\epsilon = G\frac{b^2}{\mu_f^2}\rho_o,$$

and

$$M = \frac{\mu_s}{\mu_f}.$$

Chapter 3
Solution for a Step Change in Skull Velocity

The governing equations derived in the previous section will be solved for a step change in skull velocity. The entire system will be considered such that when time is started, $t = 0$, the skull will be given a velocity of V_s. Due to inertia, the fluid, plate, and gel material will begin at rest at time zero and eventually be accelerated to the skull velocity. Since however, we measure our velocities with respect to the skull, and the fluid compartment is a closed capsule of equal density material, the effects may be thought of as the plate being given a step change in velocity equal, *but opposite*, to that of the skull, while the skull and surrounding gel and fluid remain at rest.

3.1 Finite Difference Solution

The solution of the govering equations will be found using finite difference analogues for the differential terms and coding the results into Fortran for solution by digital computer. The solution space; which extends spatially from the skull-gel interface, $y = 0$, up through the plate, $y = P$, to the fluid- skull boundary, $y = Q$, and includes time from $t = 0$ to $t = \infty$ is shown in figure 3–1. This solution space is divided by discrete time and spatial steps Δt and Δy.

It is worth noting that the model was designed for the general case where Δy for the gel and for the fluid could be different. While the computer code still maintains the ability to keep separate values, in practice, this feature was never used in such a way as to justify separate values for solid and gel. Therefore, the following derivations will consider a uniform Δy. In addition, all results presented will have $\Delta y = \Delta y_s = \Delta y_f$.

Also, the velocities of fluid, plate, and gel will be no longer designated by the separate variables $\bar{u}$, $\bar{v}$, and $\bar{w}$, but rather by the single variable $U_{i,n}$. One may acertain which material the velocity represents by the spatial subscript i.

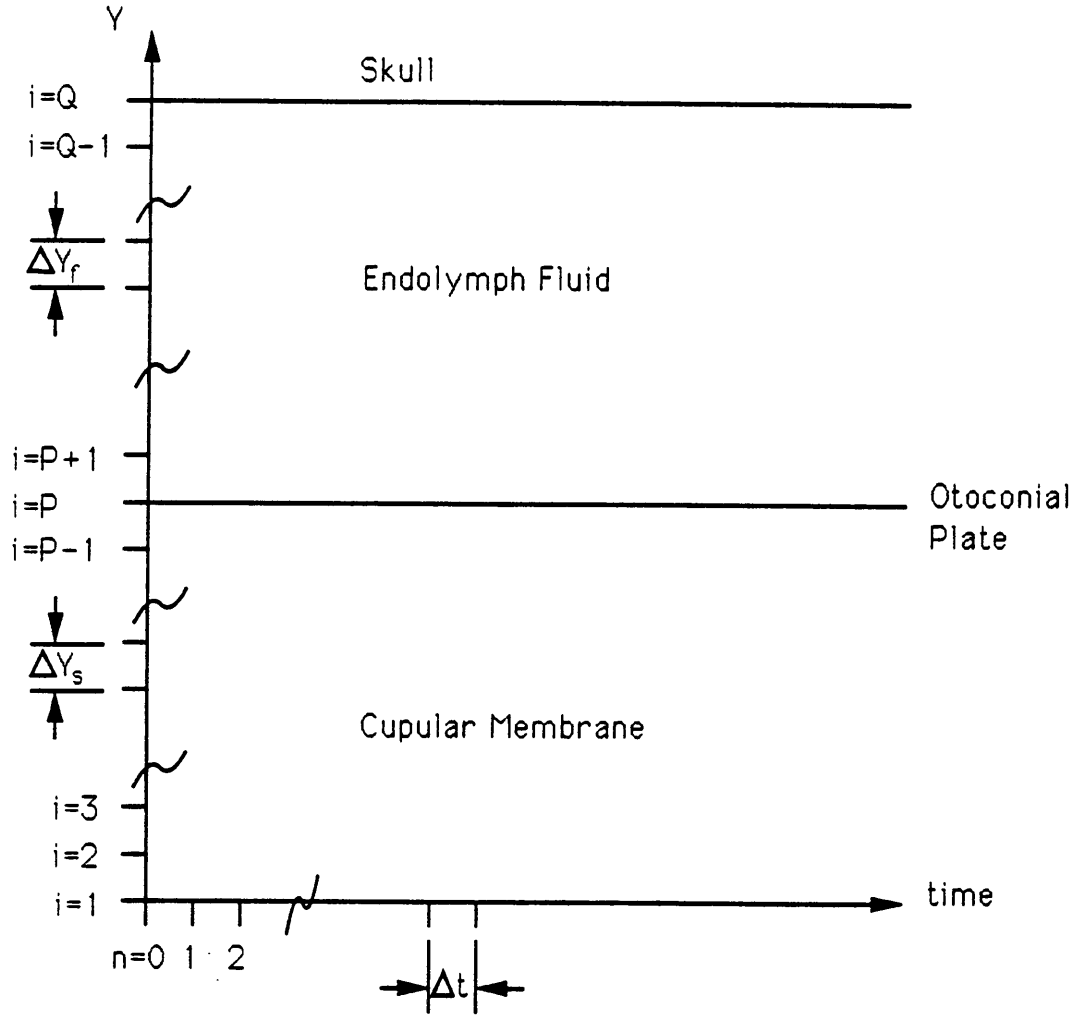

Figure 3-1: Solution Space for Numerical Model

3.1.1 Time and Space Derivative Analogues

Solution involved using the implicit method, which gives unconditional stability and first order accuracy on first order time derivatives. The derivatives for the terms in the differential equations are found by the changes in the values of these parameters at node points at, or close to the point in question. The graphical representation of this method is shown in figure 3–2. The first time derivative is defined as

$$(\frac{\partial U}{\partial t})_{i,n+1} = \frac{U_{i,n+1} - U_{i,n}}{\Delta t} + O(\Delta t),$$

and the first and second order space derivatives are

$$(\frac{\partial U}{\partial y})_{i,n+1} = \frac{U_{i+1,n+1} - U_{i-1,n+1}}{2\Delta y} + O(\Delta y^2)$$

and

$$(\frac{\partial^2 U}{\partial y^2})_{i,n+1} = \frac{U_{i+1,n+1} - 2U_{i,n+1} + U_{i-1,n+1}}{\Delta y^2} + O(\Delta y^2).$$

Spacial derivatives for displacements follow the same formulas as above only substituting δ for U.

3.1.2 Displacement Calculations

In order to calculate the displacement, δ, we used a variant of Simpson's rule. The displacement at all points was calculated using velocities from present and the two previous time steps, along with the previously calculated displacement from two time steps back according to the formula,

$$\delta_{i,n+1} = \delta_{i,n-1} + \frac{1}{3}(U_{i,n+1} + 4U_{i,n} + U_{i,n-1})\Delta t.$$

The method is graphically shown in figure 3–3.

3.1.3 Finite Difference Governing Equations

These analogues were substituted into the governing differential equations and manipulated algabraically so as to separate unknown from known quantities, or $n+1$ time subscripts from n, $n-1$, etc. subscripts. The finite difference equations then become for the fluid,

$$-U_{i-1,n+1} + (R\frac{\Delta y^2}{\Delta t} + 2)U_{i,n+1} - U_{i+1,n+1} = R\frac{\Delta y^2}{\Delta t}U_{i,n},$$

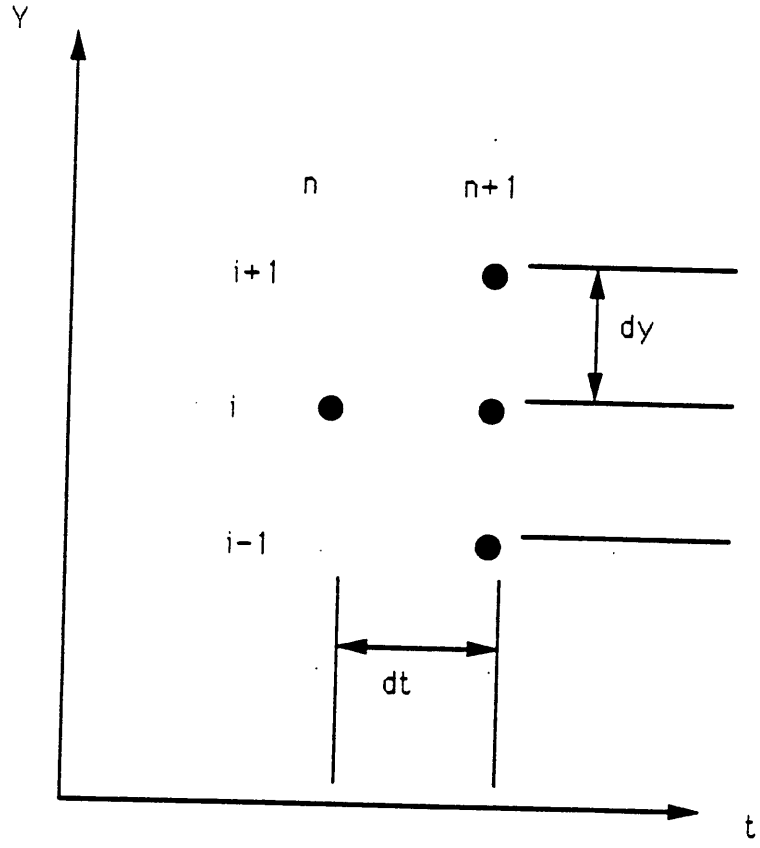

Figure 3-2: Grid points used for implicit solution

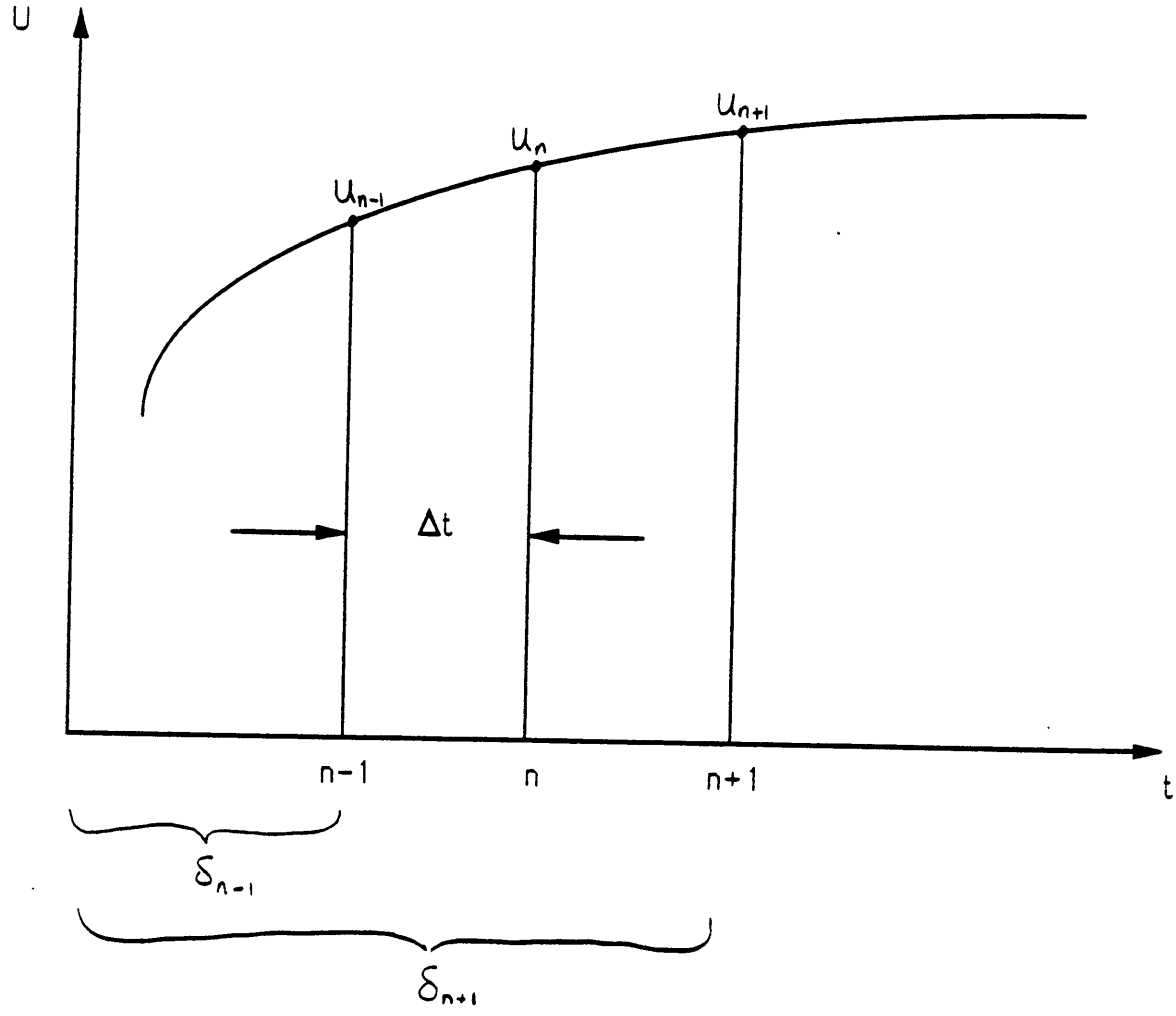

Figure 3-3: Graphical Example of Displacement calculations

for the plate,

$$(M+\epsilon\Delta t-1)U_{i-1,n+1}+2\frac{\Delta y}{\Delta t}U_{i,n+1}-(M+\epsilon\Delta t-1)U_{i+1,n+1}=2\frac{\Delta y}{\Delta t}U_{i,n}-\epsilon(\delta_{i+1,n}-\delta_{i-1,n}),$$

and for the gel,

$$-(\epsilon\Delta t+M)U_{i-1,n+1}+(R\frac{\Delta y^2}{\Delta t}+2\epsilon\Delta t+2M)U_{i,n+1}-(\epsilon\Delta t+M)U_{i+1,n+1}=$$
$$R\frac{\Delta y^2}{\Delta t}U_{i,n}+\epsilon(\delta_{i-1,n}-2\delta_{i,n}+\delta_{i+1,n}).$$

For all points $i < P$, the solid governing equation was used. For all points where $i > P$, the fluid governing equation was used.

For the point, $i = P$ however, an extra step was required. Point P in our solution space is not only the plate, but the boundary of the gel and the boundary of the fluid. In actuality, the plate equation is a boundary condition for the fluid equation and the solid equation. Therefore, we treat the formulation at $i = P$ as we would in a problem with a mixed boundary condition. This is slightly different from the typical problem because the boundary equation is inside of the field in question, rather than at the boundaries.

In the typical mixed boundary condition problem, the equation used at the boundary is determined by the governing equation and the boundary equation, both applied at the boundary. This gives rise to an imaginary point located one node from the boundary in the opposite direction of the field. The governing equation may be solved for this imaginary point. This result is substituted into the boundary equation in order to eliminate the imaginary point.

In this problem we need to know the value of the velocity at both the boundary (the plate), and at one node point from the boundary on both sides (the fluid and the solid). We solve the gel equation for the point U_{P+1}, which is its imaginary point. We then solve the fluid equation for the point U_{P-1}. Then we substitute the result of each of these equations into the plate equation, for U_{P+1} and U_{P-1}, respectively. This result is the proper formula to be used at $i = P$. Manipulating the result so that all unknowns are on the left hand side results in

$$-(1+\frac{\Delta y_s}{\Delta y_f})U_{P+1,n+1}+(R\frac{\Delta y_f^2+\Delta y_s^2}{\Delta t}+4+2\epsilon\Delta t+4\frac{\Delta y_s}{\Delta t})U_{P,n+1}$$
$$-[(1-\frac{\Delta y_s}{\Delta y_f})+2+2\epsilon\Delta t]U_{P-1,n+1}$$
$$=R\frac{\Delta y_f^2+\Delta y_s^2}{\Delta t}+2\frac{\Delta y_s}{\Delta t})U_{P,n}-2\epsilon(\delta_{P,n}-\delta_{P-1,n}).$$

The boundary condition matching is, in actuality, physically matching the shear stresses between the three equations. To neglect this step would result in discontinuities within the velocity field. When the model was run with only the plate equation used at $i = P$, the plate was the only part of the model that experienced significant movement. It is worth note that the composite equation found for $i = P$ can be derived much quicker by simply adding the solid, plate, and fluid equations together, and setting $i = P$.

3.1.4 Solution Strategy

Now that we have the equations we will solve them by establishing the initial condition that all relative velocities are zero, except for the plate which is given a velocity of $(1 - R)$. All initial displacements are set to zero. We couple these with boundary conditions of zero velocity and displacement at the skull/gel interface, and at the distant skull/fluid interface.

The solution to the family of equations is

$$[C_{i,j}][U_i] = [D_j],$$

where $[C_{i,j}]$ is a tri-diagonal matrix whose values are found in the above equations. The solution to the above equation is found by using the Thomas algorithm [14]. From this we obtain the next values of velocity, we then solve for displacements, then move ahead one more time step and repeat the procedure. Figure 3–3 is a flow chart explaining this problem solving technique.

3.2 Validation

The model was created such that the effects of fluid viscosity, gel viscosity, and gel elasticity could be independantly removed. The parameter M can be taken to zero, thereby removing the effects of solid viscosity. The parameter ϵ can also be made zero which removes the effects of gel elasticity. Finally, a parameter K was introduced in front of every term caused by the gel viscosity. Hence, when K is unity we have a case where the fluid is viscous, while if we set K to zero, the fluid viscosity is removed and we have a "no fluid" model. K is essentially an on/off switch for fluid viscosity. By independently setting these three parameters, we can recreate earlier work which neglected one or more of these characteristics and compare results, as well as compare the effects of each part separately with our expectations.

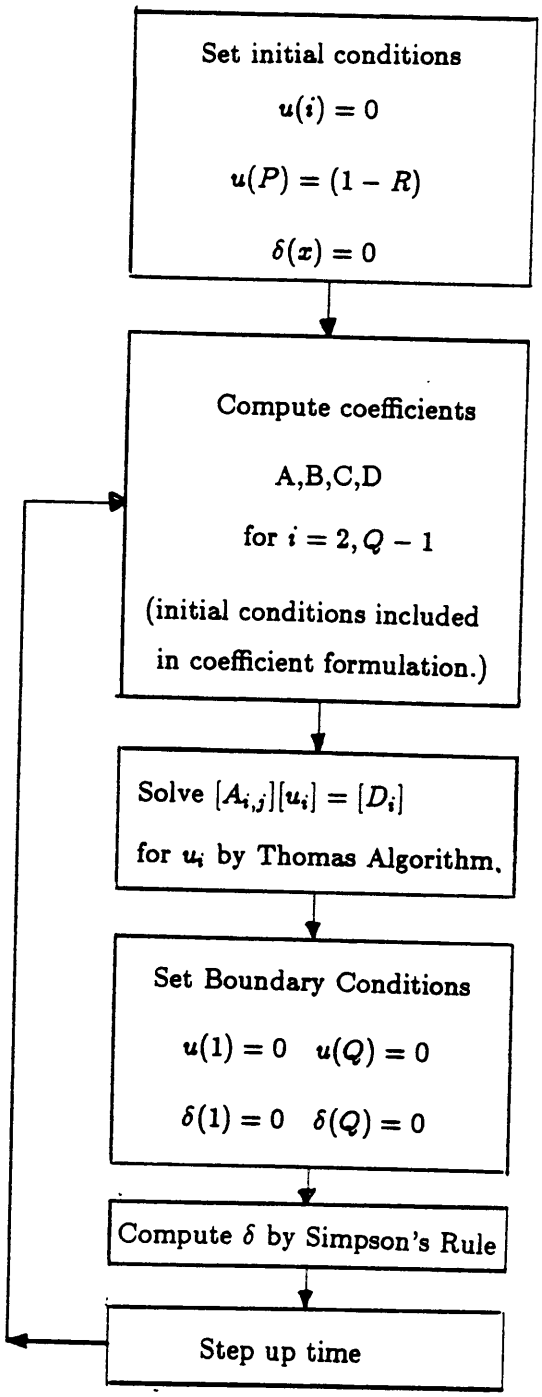

Figure 3-4: Flow Chart Of Problem Solving Technique

By removing both gel elasticity and fluid viscosity, we have the classical flow problem which has been solved analytically by Couette. The results of the model are consistent with this. With the gel modeled as a viscous fluid and the effects of the endolymph fluid viscosity removed, as time grows, $t \to \infty$, the displacement also grows indefinitely, $\delta \to \infty$. As the elasticity is slowly added, the displacements begin to become finite, which is expected.

Also by removing the gel viscosity, we can recreate the results seen by the elastic-only gel work done by Grant, Best, and LoNigro [7].

Chapter 4
Results

The effects of each of the nondimensional parameters ϵ, R, and M were studied by varying one while holding the others at probable values. The parameter which is best estimated probably is R which is the ratio of the fluid and gel densities to the density of the otoconial membrane. The calcium carbonate crystals have an approximate density value of $2.71 gm/cm^3$ while both the gelatinous membrane that makes up the cell layer and the matrix for the otoconial membrane and the endolymph fluid have been measured at $1.0 gm/cm^3$. Hence, the value for R must be between .35 and 1. More significantly, the work of Steinhausen [12] puts the specific weight of the otolith at between 1.32 and 1.39. This translates to an R value of between 0.76 and 0.72. In order to investigate the effects of the system values were run from 0.25 to 0.9. Plate displacement versus time is shown for different values of R in figure 4–1.

Notice that as R increases, displacement decreases, however the time needed to reach the maximum displacement remains nearly the same. Other than this, there is no effect on the curves. R only effects the amplitude. This is expected since the displacement is driven by the difference in densities. As R approches one, the density of the plate equals that of the fluid and no perturbation of the otolith is possible.

The value of ϵ, which represents nondimensionalized elasticity, could be varied greatly. Values approaching zero were studied as well as values that drove the system so elastic that it oscillated. Since the system is generally accepted to be overdamped, values of ϵ that cause oscillation shall constitute the upper limit of the investigation. For short times, there was little difference between cases of zero elasticity and values on the order of magnitude of 10^{-2}, while oscillation became obvious between ϵ values of 1 and 10. Grant, et. al. [1984] put "best guess" parameters for values that make up ϵ and arrived at a value of around 0.028. However, many of the values used are quite unstudied and require extrapolation from known values of other biomaterials. All in all, values of ϵ were seriously considered ranging from 0.002, which gave the same response as $\epsilon = 0.0$, to 10, which would cause the

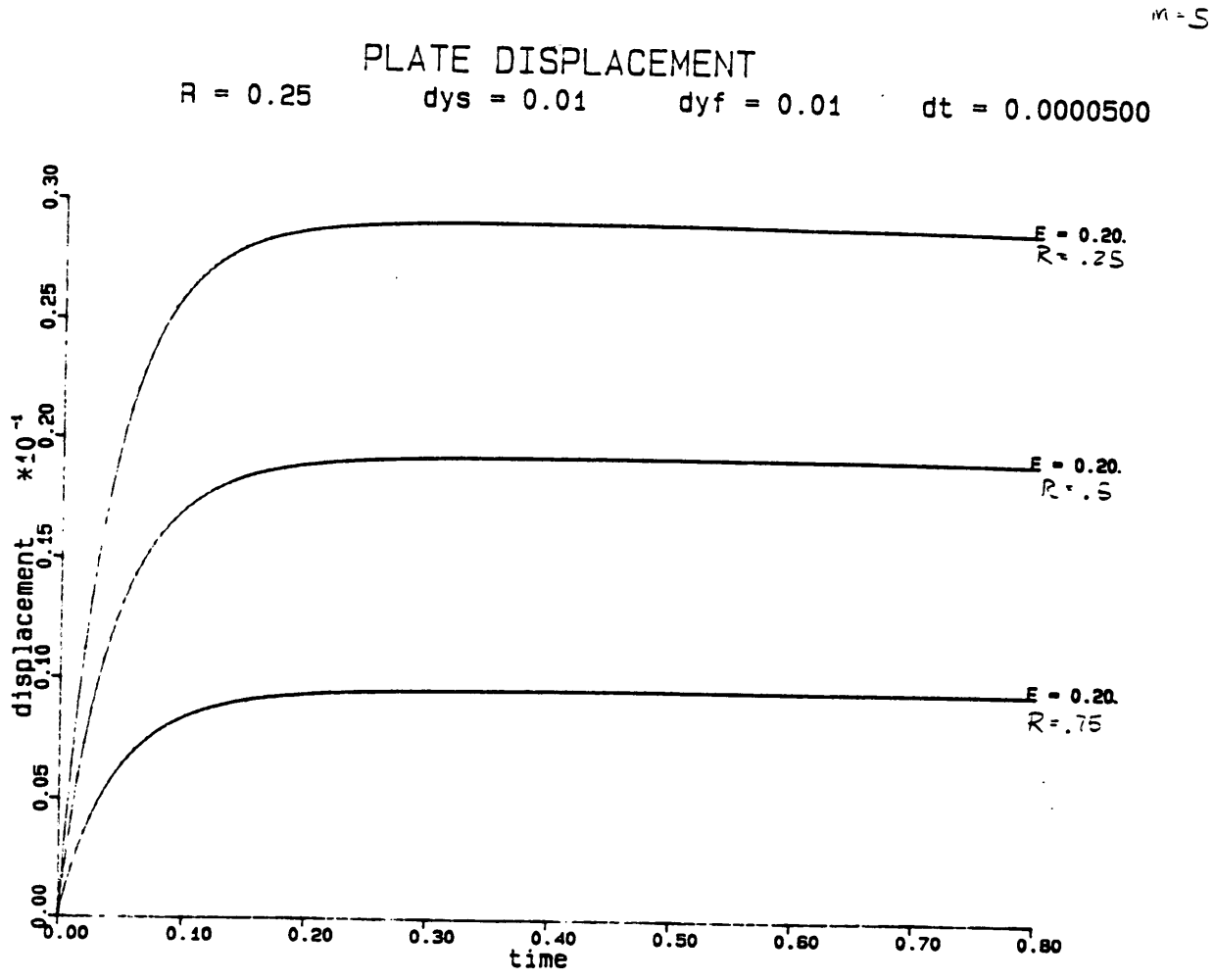

Figure 4-1: Plate displacements for different R values

system to oscillate noticeably. Plate displacement versus time is shown in figure 4–2, for various ϵ values from 0 to 5. Also a case of plate oscillation is shown in figure 4–3.

Finally the third parameter, M, which is the ratio of the gel viscosity to fluid viscosity was investigated. By increasing M, the gel viscosity increases which slows down plate velocities. This has two effects. First, the higher M values cause a smaller maximum displacement. Secondly, the higher the M values, the slower the plate displacement returns to zero after a displacement– in essence, damping out the system. Plate displacement versus time for various values of M are shown in figure 4–4.

Another input to the model regards the relative sizes of the gel layer and the fluid layer. The height of the gel is given by $h_p = (P-1)\Delta y$. Thus by increasing P, we increase the gel height. Similarly, the fluid height is given by $h_q = (Q-P)\Delta y$ and the height is controlled by regulating Q. P was given the value of 21 for our analysis since it provided a smooth curve in the displacement and velocity curves.

The proper value of Q caused some reflection during the solution process. It was originally assumed that the order of magnitude difference between the otolith height and the fluid height, would suggest an infinite fluid layer, while modeling the system. However, this analysis showed significant flow at this upper boundary. Since the upper boundary was held still, this shear traveled back down through the fluid, impeding plate motion slightly. In order to match some of the previous work by Grant, Best, and LoNigro [7], Q had to be set above 2000 spatial steps. However, for the results presented here Q was set at 1021 since this provided dimensional consistency with the anatomy of the otoconium.

Another interesting result was observed when the velocity profiles of the cupular membrane were observed. Figure 4–5 shows these profiles for different times in the application of a step change in skull velocity. At the earliest times, the profiles display an exponential curve, which shallows out to linear by the time the maximum displacement is reached. This seems to imply that the membrane is in simple shear after it reaches maximum displacement.

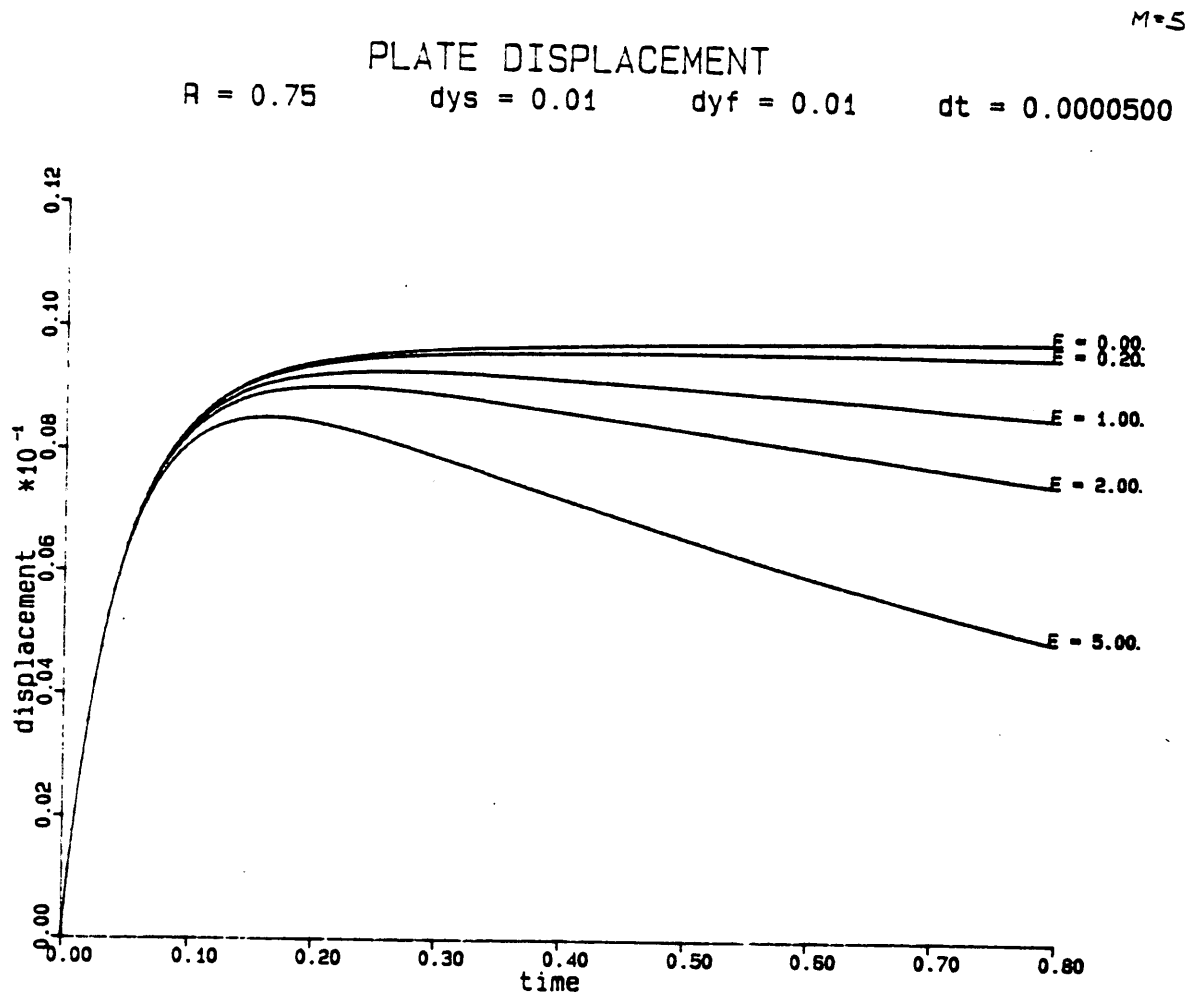

Figure 4-2: Plate Displacement verses time for varying values of ϵ

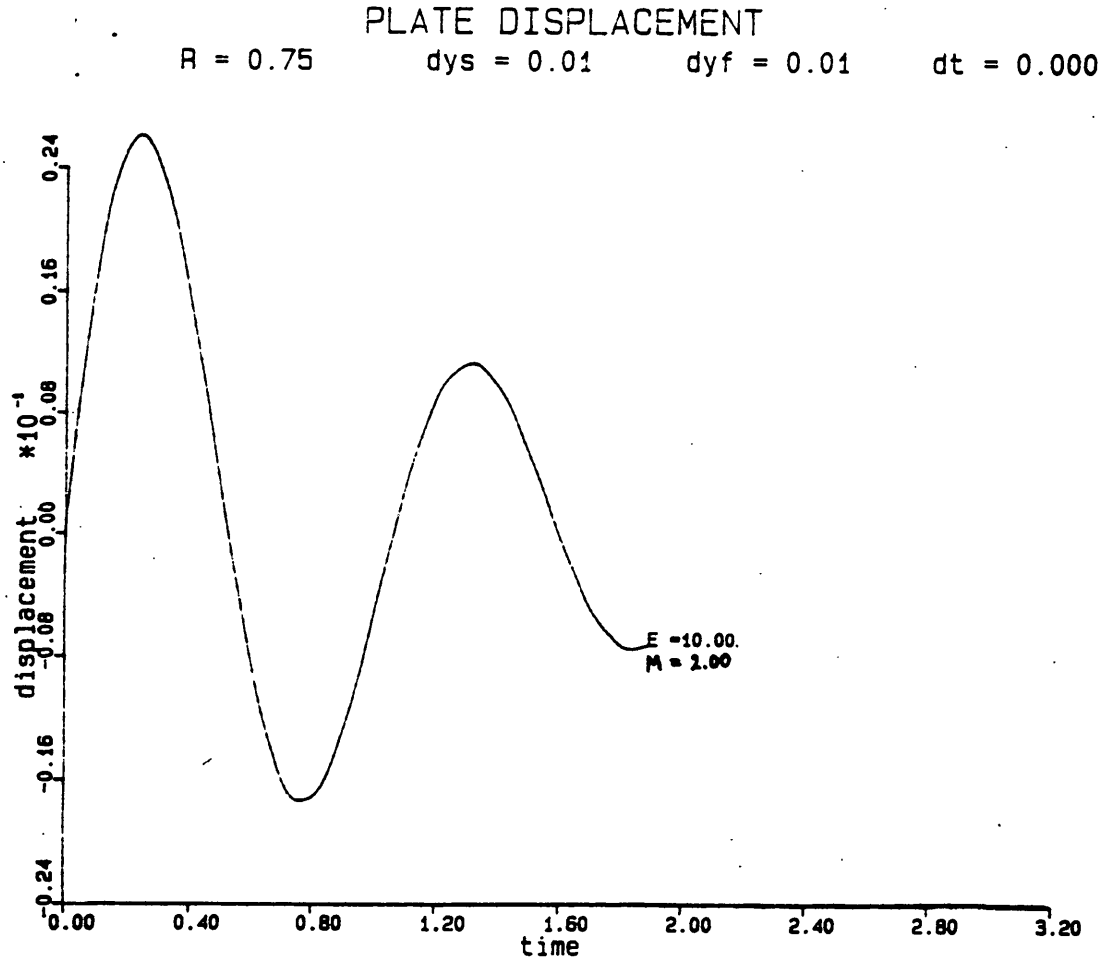

Figure 4-3: Plate Displacement for case of oscillation.

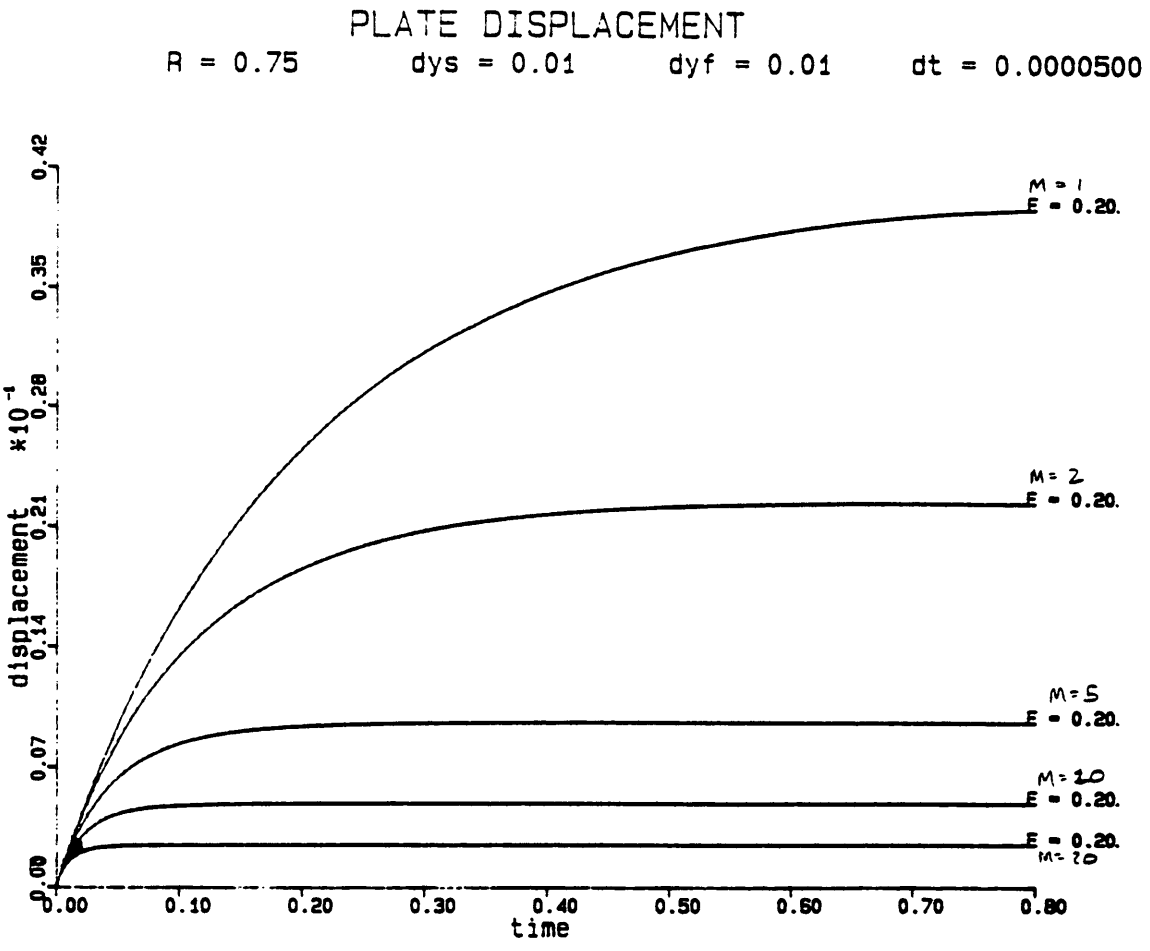

Figure 4-3: Plate Displacement verses time for various values of M

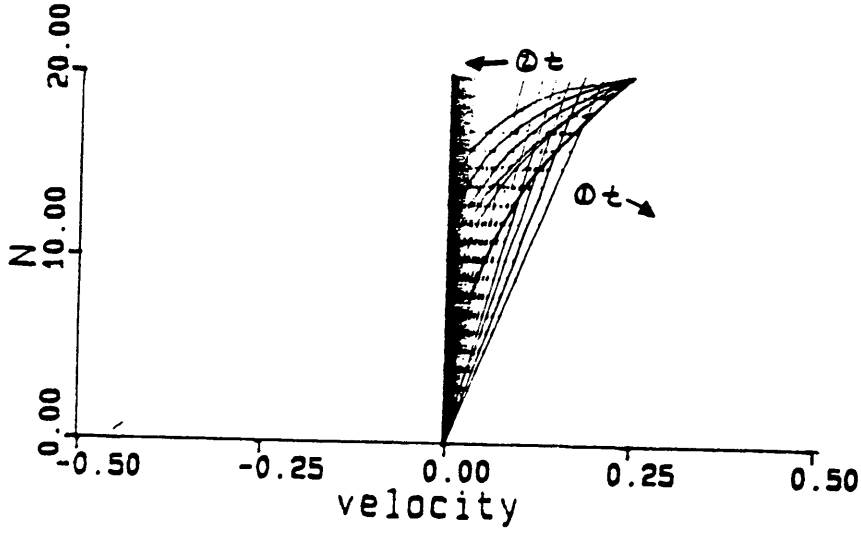

Figure 4-5: Velocity profiles for the cupular membrane

Chapter 5
Discussion

The dimensionless displacement and time must be converted back to real length and time so that they may be compared to physically observed results. From inverting the results of nondimensionalization we get

$$\delta = [\frac{V\rho_o b^2}{\mu_f}]\bar{\delta}$$

and

$$t = [\frac{\rho_o b^2}{\mu_f}]\bar{t}.$$

Accepted values for the above parameters are considered to be

$$\rho_o = 1.35gm/cm^3,$$

$$b = 15\mu m,$$

and

$$\mu_f = .85cp.$$

The characteristic velocity is taken to be 1 m/s. The results of this indicate that

$$\delta = 3.57 \times 10^{-4}\bar{\delta} \quad \text{meters}$$

and

$$t = 3.57 \times 10^{-4}\bar{t} \quad \text{seconds.}$$

We can get a reasonable value for the elasticity ϵ by observing the steady state case of an otolith under a constant acceleration. The constant acceleration of gravity will be used. Here the governing equation for the plate loses all transient terms and we are left with the acceleration term equaling the elastic term,

$$(1 - R)[-\bar{g}_x] = -\epsilon\frac{\partial\bar{\delta}}{\partial\bar{y}}.$$

We note from earlier observations that for long time solutions, of which this certainly is, the gel is in simple, linear, shear. Hence,

$$\frac{\partial \bar{\delta}}{\partial \bar{y}} = \frac{\bar{\delta}_p - \bar{\delta}_o}{\bar{y}_p} = \bar{\delta}_p,$$

because $\bar{\delta}_o = 0$ and $\bar{y}_p = 1$, as the gel height is nearly b. Hence, we can solve for ϵ,

$$\epsilon = (1 - R)\frac{\bar{g}_x}{\bar{\delta}_p}.$$

We can now place ϵ between 0.3 and 0.075, when we take R to be between 0.5 and 0.75, and the displacement due to one g to be 2 to 4 μm which is given by Goldberg [4].

By clinical observation, we know that the response of the otolith can be described as an inverse exponential climb in a very short time followed by an inverse exponential decay. Mathematically the system can be described by the linear system model,

$$\delta = \delta_{max}(e^{-\frac{t}{T_l}} - e^{-\frac{t}{T_s}})$$

where δ_{max} is the maximum plate displacement. T_l and T_s are the long and short time constants respectively, after Grant and Best [9]. This matches the quick displacement of the plate followed by a slow elastic return seen both in real life and our model.

Observed values for the time constants are needed to bracket values of elasticity and viscosity in our model. The long time constant is given by Meiry [10] and Young et. al. [16] , as well as several others, to be 10 seconds. This was determined by perception of motion decay. These authors also support a short time constant of 0.66 seconds which will not be used, since the start of perception of motion is highly dependent upon nerve speeds and not upon the mechanical transduction.

Work by Goldberg and Fernandez [6] which concentrated on the signals of afferent nerves originating in the otoliths cite a short time constant of 16 milliseconds. Although better, this is still slowed by neural transmission. The short time constant may well be assumed to be on the order of a tenth of a millisecond.

We have come to the point now where we have only one parameter to vary, and two observations (the long and short time constants) to satisfy. When M is given a value between 5 and 15 we note that the short time constant is on the order of 100 μs as was expected. However the value for the long time constant is too small, over two orders

of magnitude below the expected value of 10 seconds. In order to see if the long time constant of 10 seconds could be reached we attempted raising M to unreasonably high numbers. This resulted in three negative results. First, the system became so viscous that the displacements began to be too small for detection. Second, the short time constant grew to unreasonable results. Third, the model began to show instabilities in both time and space that became significant at values of M above 200. By extrapolating the data from these earlier points it is estimated that the long time constant would approach 10 seconds as M was around 2000-3000.

However, recent conversations with Goldberg [5] indicate that the long time constant may be an artifact, rather than a true mechanical delay. While this information may help these results some, it is doubtful that it could correct the two order of magnitude discrepancy. An eye must be kept on this debate however, since the long time constant should remain a relevant check point for future analysis.

Results at this point seem to indicate an M value that varies with strain rate. M should be between 5-15 to satisfy the short time response, but on the order of magnitude of thousands to satisfy a long time response characterized by $T_l = 10s$, or at least hundreds to satisfy a reasonably smaller $T_l = 1s$.

In summary, reasonable values of R are close to 0.75. ϵ has been bracketed between 0.3 and 0.075, with the lower values appearing more relevant. Although a single value for M is not a true representation of its behavior, when the long time response is ignored, values between 5 and 10 fit expected short time response.

Chapter 6
Conclusions

This model provides good results in many areas, while falling short at mimicking the long time response. Most notably, the deflections are correct and adaptable to variations in viscosity in both gel and fluid, as well as gel elasticity.

The greatest success of this work is the ability of the model to have increased elasticity compared to the purely elastic models of Grant and Best, and maintain reasonable displacements. The higher elasticity values correspond to expected values of ϵ. The model also shows that the same value of ϵ can maintain reasonable deflections under both steady-state conditions and dynamic conditions.

Also the conclusion that M is highly strain dependent is probably an indication of the strain dependency of the endolymph fluid viscosity, μ_f, and of the gel viscosity, μ_s. The endolymph viscosity probably increases as strain rate increases causing a corresponding drop in M. While some consider the endolymph to be a Newtonian fluid [11], the presence of protein in solution lends strong credibility to the assumption of a non-Newtonian endolymph. Also, the gel viscosity would probably decrease as strain rate decreases making the gel behave as a pseudoplastic fluid. This would also contribute to a drop in M as strain rate increases.

Further work should most certainly include the adaptation of a generalized Kelvin model for the viscoelastic gel layer. This could provide a gel that has the low viscosity needed at short times to get a noticable displacement and quick response, yet give a high viscosity for later times when the exponential decay should be slower. Also worthy of further study is the effects of "holes" in the bottom layers of the gel membrane.

Already this model offers some insight into the mechanical properties, and methods for modeling, similar membranes found in the inner-ear and elsewhere in the body. Most notably, these results should be relevant to research on material response in the semicircular canals and the cochlea.

References

[1] Best, W. A., "A Numerical Model for the Dynamic Response of the Human Otolith Organs", Masters Thesis, Virginia Polytechnic Institute and State University, June 1984.

[2] Carnahan, B., H. A. Luther, and J. O. Wilkes, *Applied Numerical Methods.* John Wiley & Sons, New York, 1969.

[3] Friedman, I., and J. Ballantyne, *Ultrastructural Atlas of the Inner Ear.* Butterworths, London, 1984.

[4] Goldberg, J.M., G. Desmadryl, R.A. Baird, and Cesar Fernandez, " The Vestibular Nerve of the Chinchilla. IV. Discharge Properties of Utricular Afferents", to be published.

[5] Goldberg, J.M., Conversation with J. W. Grant. October 1989.

[6] Goldberg, J. M., and C. Fernandez. "Physiology of peripheral neurons innervating otolith organs of the squirrel monkey. III. Response dynamics." *J. Neuralphysiol.* 39:996–1008, 1976.

[7] Grant, J.W.,W.A. Best, and R. LoNigro,"Governing Equations of Motion for the Otolith Organs and Their Response to a Step Change in Velocity of the Skull." *Journal of Biomechanical Engineering.* 106:302–308, 1984.

[8] Grant,J.W. and W.A. Best,"Mechanics of the Otolith Organ— Dynamic Response", *Annals of Biomedical Engineering.* 14:241–256, 1986.

[9] Grant,J.W. and W.A. Best,"Otolith Organ Mechanics: Lumped Parameter Model and Dynamic Response", *Aviation, Space and Environmental Medicine* 970–976, October 1987.

[10] Meiry, J. L. "A revised dynamic otolith model." *Aerospace Med.* 39:606-608, 1968.

[11] Steer,R. W.,Jr. "The Influence of Angular and Linear acceleration and Thermal Stimulation on the Human Semicircular Canal." Sc. D. Thesis, M.I.T., 1967.

[12] Steinhausen, Wilhelm, "Concerning the Forces Released by the Otoliths", *Pflugers Arch. f. d. ges. Physiol.* 235:538-544, 1934–35.

[13] Swift, G. W., Class notes from E. S. M. 5012, Virginia Polytechnic Institute and State University, Winter 1988.

[14] Von Rosenberg, D. U., *Methods for the Numerical Solution of Partial Differential Equations*, p. 113. Gerald Farrar & Assoc., Inc., Publishing Division, Tulsa, 1969.

[15] Wilson, V.J. and G. M. Jones, *Mamillian Vestibular Physiology*,Chapters 1–3, Plenum Press, New York, 1979

[16] Young, L. R., et. al. "Ocular torsion on earth and in weightlessness." *Ann. N.Y. Acad. Sci.* 374:80-92, 1981.

Appendix A: Computer Code for Otolith Model

```
      program wflim
C
      dimension U(1200),UPN(1200),UN(1200),delta(1200),deltpn(1200)
      dimension A(1200),B(1200),C(1200),D(1200),Beta(1200),Gamma(1200)
      real M,K
      integer P,Q
      character*24 fname
      common //n,t,dt,u,delta,P ,Q
C
      open(3,file='otov.in',status='old')
      read(3,*)
      read(3,*) fname
      read(3,*)
      read(3,*) dt,dys,dyf
      read(3,*)
      read(3,*) E,R,k,M
      read(3,*)
      read(3,*)P,Q
      read(3,*)
      read(3,*) printstep,tmax
      close(3)
C
      open(7,file=fname)
      write(6,23) E,R,K,M,dys,dyf,dt,P,Q
      write(7,23) E,R,K,M,dys,dyf,dt,P,Q
 23   format(5x,'E =',f7.4,5x,'R =',f5.2,5x,'K =',
     1    f5.2,5x,'M =',f5.2,/,5x,'dys =',f5.2,5x,
     2    'dyf =',f5.2,5x,'dt =',f10.7,/,5x,'P =',
     3    i3,5x,'Q =',i4)
C
      dydtr=dys*dys*r/dt
      edt=e*dt/3.0
      edtdy=e*dt/dys/2.0
      dtdy=dt/dys/2.0
      dy2=dys*dys
C
      tprint=dt*printstep
      tpindx=tprint
C
      U(P)=(1.0-R)
C
      call printdat()
C
      do 1000 n=1,100000
        t=t+dt
C
```

```
        a(2)=0.
        b(2)=dydtr+edt*6.+2.*m
        c(2)=-(3.*edt+m)
        d(2)=dydtr*u(2)+e*(delta(1)-2.*delta(2)+delta(3))
        do 200 i=3,p-1
          a(i)=c(2)
          b(i)=b(2)
          c(i)=a(i)
          d(i)=dydtr*u(i)+e*(delta(i+1)-2.*delta(i)+delta(i-1))
 200    continue
        a(p)=-(k*(1.-dys/dyf)+2.*m+6.*edt)
        b(p)=r/dt*dyf*dyf+dydtr+2.*k+6.*edt+2.*m+1./dtdy
        c(p)=-k*(1.+dys/dyf)
        d(p)=(r/dt*dyf*dyf+dydtr+1./dtdy)*u(p)-2.*e*(delta(p)-
     1     delta(p-1))
        do 250 i=p+1,q-1
          a(i)=-k
          b(i)=r*dyf*dyf/dt+2.*k
          c(i)=-k
          d(i)=r*dyf*dyf/dt*u(i)
 250    continue
        c(q-1)=0.
c thomas algorithm
        beta(2)=b(2)
        gamma(2)=d(2)/b(2)
        do 300 i=3,q-2
          beta(i)=b(i)-a(i)*c(i-1)/beta(i-1)
 300      gamma(i)=(d(i)-a(i)*gamma(i-1))/beta(i)
        un(q-1)=gamma(q-1)
        do 400 i=q-2,2,-1
 400      un(i)=gamma(i)-c(i)*un(i+1)/beta(i)
        do 500 i=2,q-1
          dummy=deltpn(i)+(un(i)+4.*u(i)+upn(i))*dt/3.
          deltpn(i)=delta(i)
          delta(i)=dummy
          upn(i)=u(i)
 500      u(i)=un(i)
c
        if(n.le.10)call printdat()
        if(t.ge.tprint)then
          tprint=tprint+tpindx
          call printdat()
        endif
        if(t.gt.tmax)stop
 1000 continue
      end
c
```

```
      SUBROUTINE PRINTDAT()
      DIMENSION U(1200), DL(1200),UF(1200)
      INTEGER P,Q
      COMMON //N,T,DT,U,DL,P,Q
      NPF=(Q-P)/20
      NP = NPF+P
      J=0
      DO 10 I=P,Q
       IF(I.EQ.NP.or.i.eq.1)THEN
        J=J+1
        NP=NP+NPF
        UF(J)=U(I)
       ENDIF
 10   CONTINUE
      WRITE (6,22)
      WRITE (7,22)
      WRITE (6,20) N,T,DT
      WRITE (7,20) N,T,DT
      WRITE (6,24) (U(I), I=1,P)
      WRITE (7,24) (U(I), I=1,P)
      WRITE (6,22)
C      WRITE (7,22)
      WRITE (6,24) (UF(I), I=1,J)
C      WRITE (7,24) (U(I), I=P,Q)
      WRITE (6,22)
      WRITE (7,22)
      WRITE (6,24) (DL(I), I=1,P)
      WRITE (7,24) (DL(I), I=1,P)
C
C          Formats
C
20    FORMAT (I10,F11.4,F15.7)
21    FORMAT (5F11.4)
22    FORMAT (' ')
24    FORMAT (5F15.8)
      END
```

Appendix B: Sample Input File for Otolith Model

```
   filename
'PVAR2.dat'
   dt    dys  dyf
 .0001   .2 .01
   E     R    K     M
  .03   0.37   1.    0.
  P     Q
 2   1003
 printstep   tmax    stretch
      100.    25.    0.
```

Appendix C: Computer Code for Displacement Plots

```
      program  dispp
C
C   this program will graphically display the results of otov using the HP plotter
C
      dimension D(23),N(23),disp(12000),time(12000)
      character*24 l1,l2,l3,l4,fname,LE,LR,LDYs,ldyf,LDT,ltime,l6,l5
      real n

C   lables for the axes
      l1='displacement'
      l2='N'
      L3='PLATE DISPLACEMENT'
      l5='time'
      l6='velocity'
C
      do 100 i=1,21
  100 N(i)=float(i-1)
C
      write(6,*) ' enter the # of files you want to plot'
      read *, nplot
      do 600 kk=1,nplot
        write(6,*) ' Enter the data file name you want to plot'
        read *, fname
        open(5,file=fname,status='old')
        read(5,10) lE,lR
        read(5,20) ldys,ldyf,ldt
        if(kk.eq.1)then
          call plots(4,3,20)
          call plot(.5,.5,-3)
C
          call symbol(2.4,7.1,.2,L3,0.0,18)
          call symbol(.9,6.8,.15,lR,0.,8)
          call symbol(2.9,6.8,.15,ldys,0.,10)
          call symbol(5.,6.8,.15,ldyf,0.,10)
          call symbol(7.,6.8,.15,ldt,0.,14)
        endif
        call plot(0.,0.,-3)
C
C plot of displacement profiles
C
        do 200 l=1,200
          read(5,30,end=500) nstep,ltime,dt
          time(l)=nstep*dt
          npts=l
```

```
            read(5,21)
            read(5,25)  (D(i),i=1,21)
            disp(1)=d(21)
            if (1.ne.1)then
             if(1.eq.2)then
              D(22)=0.
              d(23)=.025
              n(22)=0.
              n(23)=10.
             endif
           endif
  200     continue
  500     close(5)
C
C plot of plate displacement vs. time
C
          call plot(0.,0.,-3)
C This program can either use manually scaled axes or have
C the "scale" function automatically do it. The one set not
C being used is commented out using asterixes (*).
C  This set of lines:
         if(kk.eq.1)then
           call scale(time,8.0,npts,1)
           call scale(disp,8.0,npts,1)
         endif
C or this
*          time(npts+1)=0.
*          time(npts+2)=.1
*          disp(npts+1)=0.0
*          disp(npts+2)=.007
C end of scaling options
        if(kk.eq.1)then
        call axis(0.,0.,15,-4,8.0,0.0,time(npts+1),time(npts+2))
        call axis(0.,0.,11,12,6.0,90.,disp(npts+1),disp(npts+2))
        endif
        call line(time,disp,npts,1,0,1)
        call symbol(999.,999.,.1,1E,0.,8)
        call plot(0.,0.,-3)
 600   continue
C
      call newpen(0)
      call plot(0.0,0.0,999)
C
   10  format(5x,a10,5x,a8)
   25  format(5f15.8)
   21  format(5(/))
   22  format(/)
   20  format(5x,a10,5x,a10,5x,a14,/)
   30  format(/,i10,5x,a4,6x,f11.7)
      end
```

The vita has been removed from the scanned document